Seaborne measurements of near infrared water-leaving reflectance: The similarity spectrum for turbid waters

Kevin G. Ruddick,[1] *Vera De Cauwer,*[2] *and Young-Je Park*

Management Unit of the North Sea Mathematical Models (MUMM), Royal Belgian Institute for Natural Sciences (RBINS), 100 Gulledelle, B-1200 Brussels, Belgium

Gerald Moore

Plymouth Marine Laboratory, Prospect Place, Plymouth PL1 3DH, United Kingdom

Abstract

Theory and seaborne measurements are presented for the near infrared (NIR: 700–900 nm) water-leaving reflectance in turbid waters. According to theory, the shape of the NIR spectrum is determined largely by pure water absorption and is thus almost invariant. A ''similarity'' NIR reflectance spectrum is defined by normalization at 780 nm. This spectrum is calculated from seaborne reflectance measurements and is compared with that derived from laboratory water absorption measurements. Factors influencing the shape of the similarity spectrum are analyzed theoretically and by radiative transfer simulations. These simulations show that the similarity spectrum is valid for waters ranging from moderately turbid (e.g., water-leaving reflectance at 780 nm of order 10^{-4} or total suspended matter concentration of order 0.3 g m^{-3}) to extremely turbid (e.g., reflectance at 780 nm of order 10^{-1} or total suspended matter of order 200 g m^{-3}). Measurement uncertainties are analyzed, and the air-sea interface correction is shown to be critical for low reflectances. Applications of the NIR similarity spectrum to atmospheric correction of ocean color data and to the quality control of seaborne, airborne, and spaceborne reflectance measurements in turbid waters are outlined.

Although ocean color remote sensing has focused primarily on visible wavelengths (400–700 nm) where photosynthetic pigments have detectable absorption features, there is a growing interest in water-leaving reflectances at near infrared (NIR) wavelengths, usually taken as the range 700–1,000 nm. There are essentially three reasons for this. First, although for atmospheric correction over clear waters the NIR water-leaving reflectance can usually be taken as zero (Gordon and Wang 1994), for turbid waters it is essential to model or estimate NIR water-leaving reflectance in order to

accurately estimate the aerosol reflectance spectrum (Moore et al. 1999). Second, the retrieval of total suspended matter (TSM) concentration in turbid waters can be more accurate for NIR wavelengths. At visible wavelengths the absorption properties of phytoplankton and dissolved or particulate yellow substance must be considered, thus complicating and potentially degrading TSM retrieval. Also, for very turbid water the relation between reflectance and TSM at visible wavelengths becomes nonlinear (Althuis and Shimwell 1995; Bowers et al. 1998; Van Der Woerd and Pasterkamp 2004) and less sensitive. Shifting to higher NIR wavelengths (Stumpf and Pennock 1989) alleviates such problems provided the water-leaving reflectance signal is strong enough to be accurately measured. Third, the retrieval of chlorophyll *a* (Chl *a*) concentration in turbid waters with high yellow substance absorption is greatly improved by using reflectances at and near the red chlorophyll absorption peak (665 nm). For example, algorithms using water-leaving reflectances at 665 and 705 nm (or similar wavelengths) are effective in high Chl *a,* turbid waters (Dekker 1993; Gitelson 1992; Gons 1999).

In contrast to the visible wavelengths, where it may be necessary to consider the absorption properties of phytoplankton, colored dissolved organic matter, and nonalgae particles, optical properties in the NIR may be considered as comparatively simple. Because of the large NIR absorption of pure seawater, this is generally the dominant absorbing component (Stumpf et al. 2002), and the effect of other absorbing components on the water-leaving reflectance can be neglected or considered as small correction terms. Moreover, the absorption of pure seawater is fairly constant in time and space (notwithstanding some temperature variation discussed later), and tabulated laboratory absorption measurements are

usually considered as applicable for all waters. Thus, the spatiotemporal variability of NIR inherent optical properties is primarily determined by a single component, the total backscatter coefficient, which is generally related linearly to TSM.

Despite this apparent simplicity of the NIR optical properties, there is a lack of measured data to substantiate and quantify assumptions used in the above applications. The inherent optical properties are normally not measured for wavelengths higher than 700 nm. For water-leaving reflectance, underwater profiling techniques cannot be extrapolated to the surface without large uncertainties in the NIR owing to the high vertical attenuation caused by seawater absorption. Both profiling and floating instruments measuring underwater suffer problems of instrument self-shading. Above-water techniques, however, do allow direct measurement of NIR water-leaving reflectance provided that the water is sufficiently turbid to give a strong signal compared with the measurement uncertainties.

Until recently only a few reports of seaborne measurements of NIR water-leaving reflectance beyond 800 nm were available, presumably because such measurements require suitable instrumentation, careful correction for air-sea interface reflection, and rather turbid water for acceptable accuracy. As examples, the above-water measurements of Han and Rundquist (1997), Forget et al. (1999), and Doxaran et al. (2002) all show spectra with a common shape in the NIR, as do the underwater measurements of Malthus and Dekker (1995). However, a precise assessment of the NIR spectral shape was not the objective of these studies, and the measurement protocols used were not well-adapted for this purpose, notably regarding the viewing geometry and sky reflectance correction for the above-water measurements. No information is given in these studies of spatiotemporal (in)variability for the NIR spectral shape, and spectra normalized by reflectance at a reference wavelength are not presented.

Sydor et al. (2002) present reflectance spectra for 400–950 nm measured underwater for various coastal and inland waters. A linear correlation is demonstrated between reflectance and $(\lambda a_w)^{-1}$, where λ is wavelength in nanometers and a_w is the pure water absorption coefficient, and the spectral shape with peak near 800 nm is seen. Although this study and others imply the existence of an approximately invariant spectral shape for the NIR water-leaving reflectance and suggest that the spectral shape depends mainly on pure water absorption and the backscattering or scattering coefficient, the possible variability of the NIR spectrum has not before been systematically investigated.

The objective of this paper is to present and analyze shipborne water-leaving reflectances for the NIR spectral range, thus providing suitable reflectance ratio input data for turbid water atmospheric correction, and to analyze the (in)variability of NIR spectral shape. Application of the results to the correction or quality control of above-water reflectance measurements is also outlined.

First, the theory relating water-leaving reflectance to inherent optical properties is briefly summarized with discussion of approximations appropriate for the NIR. Radiative transfer simulations are then used to assess the validity of the resulting theoretical model. Next the measurement method for above-water reflectance measurements is described, including an estimation of measurement uncertainties. Water-leaving reflectance data are presented for a number of cruises carried out in the southern North Sea for a range of conditions. These data are used to establish a globally applicable "similarity" NIR reflectance spectrum and to estimate key reflectance ratios needed for turbid water atmospheric correction of ocean color sensors such as SeaWiFS, MODIS, GLI, and MERIS. The consistency of these data with established reflectance models and laboratory data for pure water absorption is assessed and factors affecting variability of the NIR reflectance spectrum are discussed. Finally, the needs for further measurement of optical properties are prioritized in terms of reducing the uncertainty in the estimates provided.

Theory and radiative transfer modeling

Definitions of reflectance—In this section the terminology used for radiometric parameters is defined. Adopting the MERIS convention, the standard satellite-derived apparent optical property considered here is the water-leaving radiance reflectance, ρ_w, as defined by:

$$\rho_w(\theta, \phi) = \frac{\pi L_w^{0+}(\theta, \phi)}{E_d^{0+}} \tag{1}$$

where L_w^{0+} is the water-leaving radiance (i.e., the upwelling radiance measured above water in the sensor viewing direction after removal of light reflected at the air-sea interface; Mobley 1994); E_d^{0+} is the downwelling irradiance; and (θ, ϕ) are the zenith and azimuth angles for the viewing direction. This reflectance quantity, also called water-leaving reflectance, is simply equal to π times the remote sensing reflectance. It was introduced for compatibility with atmospheric reflectances (Gordon and Wang 1994). The subsurface irradiance reflectance, R^{0-}, is defined as

$$R^{0-} = \frac{E_u^{0-}}{E_d^{0-}} \tag{2}$$

where E_u^{0-} and E_d^{0-} are the upwelling and downwelling irradiance just beneath the air-sea interface, respectively. To relate radiance to irradiance, the Q factor is defined as

$$Q(\theta, \phi) = \frac{E_u^{0-}}{L_u^{0-}(\theta, \phi)} \tag{3}$$

where L_u^{0-} is the upwelling radiance just below the air-sea interface. The below- and above-water upwelling radiances are related by (Gordon and Morel 1983)

$$\frac{L_w^{0+}}{L_u^{0-}} = \frac{1 - \rho_F}{n_w^2} \tag{4}$$

where ρ_F is the Fresnel reflectance for upwelling radiance from water to air, and n_w is the refractive index of water. The below- and above-water downwelling irradiances are related by (Morel and Gentili 1996)

$$\frac{E_d^{0+}}{E_d^{0-}} = \frac{1 - \bar{r}R^{0-}}{1 - \bar{\rho}} \tag{5}$$

where $\bar{r}$ is the coefficient of reflection of upwelling irradiance from water to air, and $\bar{\rho}$ is the reflection coefficient for downwelling irradiance from air to water. Combining Eqs. 1–5 gives

$$R^{0-} = \frac{Q}{\pi} \frac{n_w^2}{(1 - \rho_F)(1 - \bar{\rho})} (1 - \bar{r}R^{0-}) \rho_w \qquad (6)$$

To simplify notation, the terms covering reflection and refraction effects at the air-sea interface can be grouped (Morel and Gentili 1996) via

$$\Re = \frac{(1 - \rho_F)(1 - \bar{\rho})}{n_w^2(1 - \bar{r}R^{0-})} \qquad (7)$$

This term $\Re$ represents reflection and refraction effects at the air-sea interface and depends primarily on the viewing zenith angle θ and sea state and weakly on the sun zenith angle θ_0. It is noted that a dependence on R^{0-} itself remains within $\Re$, although this will be negligible for small reflectances. Using Eq. 7, Eq. 6 can be rewritten:

$$R^{0-} = \frac{Q}{\pi \Re} \rho_w \qquad (8)$$

Theoretical approximation of the NIR water-leaving reflectance spectrum—In this section the wavelength variation of water-leaving reflectance in the NIR will be explained and a first approximation will be made to provide a simple intuitive basis. Improvements to this first approximation are considered in the following section. A useful first approximation (later refined) to the NIR water-leaving reflectance spectrum can be achieved from the assumptions (Ruddick et al. 2000) given in the following Eqs. 9–13.

Using the model of Morel and Gentili (1996) but expressing for the water-leaving reflectance ρ_w rather than the subsurface irradiance reflectance, the reflectance can be related to the inherent optical properties (IOPs); the total absorption coefficient, a; and the total backscatter coefficient, b_b, by

$$\rho_w(\lambda) = \frac{\pi f' \Re}{Q} \frac{b_b}{a + b_b} \qquad (9)$$

where f' varies (Morel and Gentili 1991; Loisel and Morel 2001; Park and Ruddick 2005) with sun zenith angle and with inherent optical properties.

The terms of Eq. 9 all contain some wavelength dependence. However, most of this spectral variability, except that of $a(\lambda)$, is small in the NIR (Gould et al. 2001) for typical remote sensing situations. Thus, the product $\gamma = \pi f' \Re / Q$ is considered to be wavelength-independent for the NIR in Eq. 9:

$$\frac{\partial \gamma}{\partial \lambda} = 0 \qquad (10)$$

The backscatter coefficient is considered negligible in comparison with the pure water absorption coefficient and is set equal to zero in the denominator of Eq. 9:

$$b_b \ll a \quad \text{and} \quad \frac{b_b}{a + b_b} \approx \frac{b_b}{a} \qquad (11)$$

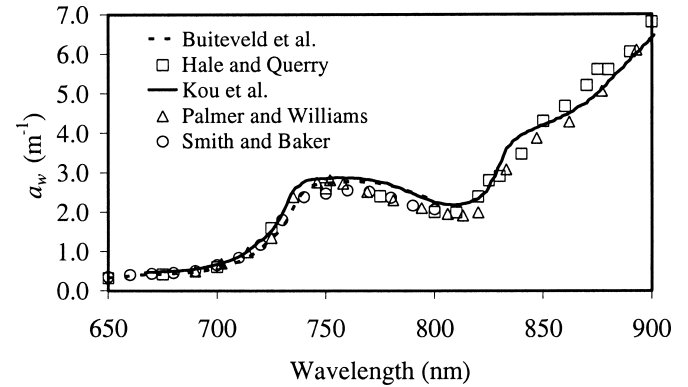The backscatter coefficient is relatively constant over

Fig. 1.   Pure water absorption coefficient as reported by Buiteveld et al. (1994), Hale and Querry (1973), Kou et al. (1993), Palmer and Williams (1974), and Smith and Baker (1981).

wavelength for limited spectral ranges and is taken as a constant in Eq. 9:

$$\frac{\partial b_b}{\partial \lambda} = 0 \qquad (12)$$

Phytoplankton, nonalgae particles (Babin and Stramski 2002), and yellow substance absorption are assumed negligible compared with pure water absorption in the NIR. Thus the total absorption coefficient in Eq. 9 can be set equal to a_w, the pure water absorption coefficient:

$$a(\lambda) = a_w(\lambda). \qquad (13)$$

Existing data for a_w spectra as measured in the laboratory are shown in Fig. 1.

The validity of the assumptions of Eqs. 9–13 is further assessed later, where better approximations are considered. However, for the present section these assumptions are supposed valid and the water-leaving reflectance can then be very simply related to pure water absorption and total backscatter by

$$\rho_w(\lambda) = \gamma \frac{b_b}{a_w(\lambda)} \qquad (14)$$

In order to consider just the shape and not the magnitude of the reflectance spectrum, the normalized water-leaving reflectance spectrum, $\rho_{wn\,780}$, is defined here by dividing the reflectance by its value at 780 nm, a wavelength where water absorption is almost independent of temperature (Buiteveld et al. 1994):

$$\rho_{wn\,780}(\lambda) = \frac{\rho_w(\lambda)}{\rho_w(780)} \qquad (15)$$

Then, according to the approximations used for Eq. 14, this normalized water-leaving reflectance spectrum is defined entirely by the pure water absorption spectrum

$$\rho_{wn\,780}(\lambda) = \frac{a_w(780)}{a_w(\lambda)} \qquad (16)$$

Apart from possible temperature variations, which are discussed later, a_w can be considered as relatively independent of region and season. The 780 nm normalized water-leaving
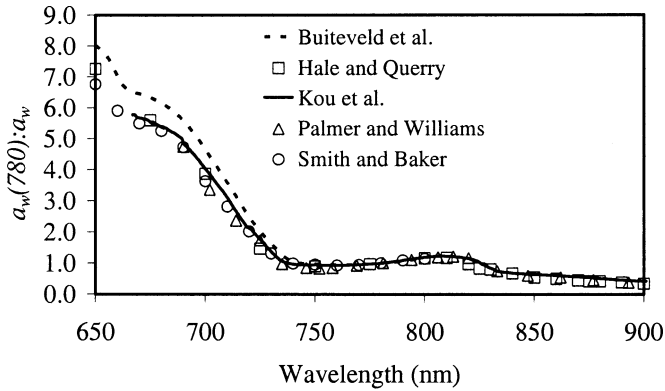
Fig. 2. $a_w(780)/a_w(\lambda)$, the reciprocal of a pure water absorption coefficient normalized at 780 nm using data from Buiteveld et al. (1994), Hale and Querry (1973), Kou et al. (1993), Palmer and Williams (1974), and Smith and Baker (1981).

Fig. 3. Normalized reflectance spectrum $\rho_{wn\,780}(\lambda)$ estimated from Eq. 18 using the pure water absorption data of Kou et al. (1993) at 22°C and with $n = 0$ compared with the same data but for $n = 1$ and with temperature adapted to 10°C.

reflectance spectrum, $\rho_{wn\,780}(\lambda)$ is, thus, globally applicable and is termed hereafter the *similarity NIR reflectance spectrum* to avoid confusion with the many other definitions for normalization of reflectances. The shape of this similarity spectrum is shown in Fig. 2 for various reported values of the pure water absorption coefficient. It is noteworthy that the differences between these published data sets for pure water absorption are both significant, if such data are used for turbid water atmospheric correction, and are not easily explainable in terms of the experimental uncertainties (Buiteveld et al. 1994).

If a reliable table of values can be established for $\rho_{wn\,780}(\lambda)$, then the water-leaving reflectance spectrum for the whole NIR range considered can be defined uniquely from a single wavelength, such as $\rho_w(780)$ (i.e., the shape of the NIR water-leaving reflectance spectrum is determined entirely by $\rho_{wn\,780}(\lambda)$, and its magnitude is determined by reflectance at a single wavelength). This magnitude is approximately proportional to the backscatter coefficient. Similarly, the ratio of any two NIR water-leaving reflectances is a constant and can be calculated directly from the similarity spectrum $\rho_{wn\,780}(\lambda)$. In the results of this study, $\rho_{wn\,780}(\lambda)$ is estimated from seaborne measurements, thus avoiding the uncertainties involved in the various theoretical approximations used here but, of course, introducing new uncertainties from the seaborne measurement method.

Theoretical variability of the NIR water-leaving reflectance spectrum—The theory given in the preceding section supporting the use of a universal similarity NIR reflectance spectrum contains a number of approximations and assumptions. Departures from this similarity spectrum can, therefore, be expected to occur (Ruddick et al. 2000) if such theory is not valid as investigated in this section.

Spectral dependence of backscatter coefficient: A wavelength-constant backscatter coefficient was assumed in Eq. 12 in order to derive Eq. 16. This can be generalized by modeling the wavelength dependence of backscatter from tripton (the dominant scattering component for highly reflective waters; Morel and Prieur 1977) by
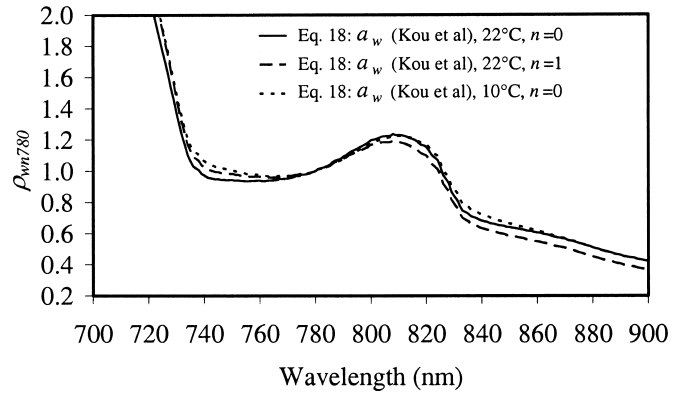
$$b_b(\lambda) = b_b(555)\left(\frac{\lambda}{555}\right)^{-n} \qquad (17)$$

where the spectral exponent n depends on particle type and size (Babin et al. 2003*a*). Although this formulation was originally developed for visible wavelengths, it is based on Mie scattering theory and should be valid also for the NIR spectral range. Thus the simpler model Eq. 16 can be generalized for $n \neq 0$ to give

$$\rho_{wn\,780}(\lambda) = \frac{a_w(780)}{a_w(\lambda)}\left(\frac{\lambda}{780}\right)^{-n} \qquad (18)$$

Few direct measurements of spectral backscatter are available (Tassan and Ferrari 1995; Whitlock et al. 1981), especially for the NIR. However, extrapolation of measurements of the scattering coefficient (Gould et al. 1999; Babin et al. 2003*a*) to the NIR and assumption of a spectrally constant scattering to backscattering ratio (at least over the limited spectral range considered) suggests that for highly scattering waters dominated by nonalgae particles, n is likely to lie within the range 0–1. $n = 1$ is shown by Sydor et al. (2002) to give good agreement for seaborne reflectance measurements in an equation equivalent to Eq. 18. The impact of variation in n on the normalized reflectance spectrum is shown in Fig. 3, where the pure water absorption data of Kou et al. (1993) is used as is currently recommended for SeaWiFS and MERIS data processing. A change in n from 0 to 1 causes a decrease/increase in $\rho_{wn\,780}(\lambda)$ for wavelengths greater/less than 780 nm of about 13% per 100 nm difference from 780 nm.

For completeness it is noted that the spectral variation of total backscatter given by Eq. 17 is not appropriate for very low tripton conditions where backscatter from phytoplankton and from water molecules may be important, giving a very different spectral variation. In the extreme case of water with no suspended particles, the total backscatter coefficient will be given by the backscatter coefficient of pure water, for which the wavelength variation can be expressed also by a power law form as Eq. 17 but with much larger $n = 4.32$ (Morel 1974). This would make a significant difference to

the spectrum $\rho_{\mathrm{wn}\,780}(\lambda)$, but this case is of little practical relevance because NIR reflectances for such clear water are generally too small (e.g., less than 10^{-4}) to be measurable.

Absorption from other water constituents: The simple theory for Eq. 18 neglected absorption from phytoplankton, nonalgae particles, and colored dissolved organic matter, assuming that total absorption is equal to pure water absorption in the NIR. The tank experiments of Lavender et al. (2005) show that reflectance is insensitive to phytoplankton for the range 700–900 nm, but not for 670 nm. The measurements of Babin and Stramski (2002) suggest that the NIR absorption by aquatic particles is very small, although the measurements of Tassan and Ferrari (2003) suggest that it may not be zero for some particles. In the absence of absolute measurements of NIR absorption, the impact of nonalgae particle absorption can only be estimated theoretically by assuming that an exponential decrease with wavelength (Bricaud et al. 1981) of slope 0.0123 nm^{-1} (Babin et al. 2003*b*) can be extended from the visible into the NIR. By adding such absorption to the denominator and numerator of Eq. 16, the impact on the similarity spectrum is found to be $<1\%$ for the spectral range 730–900 nm for a nonalgae particle absorption coefficient of 1 m^{-1} at 443 nm. The impact of colored dissolved organic matter absorption is much smaller ($<0.25\%$ at 730 nm) for an equivalent absorption coefficient of 1 m^{-1} at 443 nm because of the greater spectral decrease (e.g., of slope 0.0176 nm^{-1}; Babin et al. 2003*b*). These estimates are not shown on Fig. 3 because they are almost indistinguishable graphically from the estimates with just pure water absorption.

Temperature dependence of pure water absorption: In the simple first order theory and for Fig. 2, the pure water absorption coefficient was assumed constant, although a temperature effect has been shown to be significant (Pegau and Zaneveld 1993) for the range 745–755 nm with a 0.36% change per 1°C at 750 nm. To the authors' knowledge the only measurements of temperature dependence of the pure water absorption coefficient for the entire 700–900 nm range have been made by Hollis (2002). Although they were made for an entirely different application (brain tissue monitoring) and at a higher temperature (28–42°C), these data are very similar to those measured in the range 700–800 nm by Buiteveld et al. (1994). Using the coefficient for temperature dependence of Hollis (2002) with the pure water absorption data of Kou et al. (1993), the impact on the similarity NIR reflectance spectrum is shown in Fig. 3. The increase of reflectance with decreasing temperature is seen most clearly at 740 and 840 nm, where a 12°C decrease gives an increase of $\rho_{\mathrm{wn}\,780}(\lambda)$ at these two wavelengths of about 9% and 6%. The variation of pure water absorption with salinity is thought to be negligible (Pegau et al. 1997).

Extremely turbid waters: The validity of the model (Eq. 9) and the accompanying approximations (Eqs. 10, 11) need to be assessed in order to evaluate the robustness that can be expected for the simple result (Eq. 18). In particular, the model (Eq. 9) and the approximation (Eq. 11) were developed for relatively low reflectances only. Moreover, the use of wavelength-independent $\mathfrak{R}$ may be dubious for high reflectances because of the dependence on reflectance given in the denominator of Eq. 7. Other models exist (Gordon et al. 1988), which include second-order $[b_{\mathrm{b}}/(a + b_{\mathrm{b}})]^2$. However, according to Whitlock et al. (1981), even the use of second-order terms may not provide a realistic approximation to the full radiative transfer problem for high $b_{\mathrm{b}} : a$. The associated assumption of Eq. 10 of wavelength-independent γ is similarly subject to some uncertainty. In order to test these assumptions more fully, particularly for extremely turbid waters, full radiative transfer simulations have been performed with the Hydrolight 4.2 software (Mobley and Sundman 2001) for the wavelengths 778.5 and 864.8 nm (central wavelengths for MERIS atmospheric correction bands) under the following conditions.

Optical properties are considered as a combination of pure sea water and nonalgae particles with TSM concentration X, which is varied over the range 0.03–316 g m^{-3}:

$$a = a_{\mathrm{w}}(\lambda) + 0.041 \text{ m}^2 \text{ g}^{-1} \times X \times e^{-0.0123 \text{ nm}^{-1} \times (\lambda - 443)} \quad (19)$$

where the absorption coefficient of water and TSM are taken from Kou et al. (1993) and Babin et al. (2003*b*) and extrapolated to the NIR, respectively, and

$$b = b_{\mathrm{w}}(\lambda) + 0.51 \text{ m}^2 \text{ g}^{-1} \times X \times \left(\frac{\lambda}{555}\right)^{-0.15} \quad (20)$$

where the scattering coefficient of water, b_{w}, and TSM are based on Morel (1974) and Babin et al. (2003*a*), respectively, and the wavelength exponent has been chosen to fit approximately the case 2 water data shown in Fig. 11 of Babin et al. (2003*a*).

The scattering phase function for pure sea water and for TSM are obtained from Einstein-Smoluchowski theory and from the average Petzold phase function (Mobley 1994), respectively.

The sky radiance distribution is simulated for a sun zenith angle of 30° by the cardiodal radiance distribution defined by Eq. 4.50 of Mobley (1994) and adjusted to give a ratio of diffuse to total sky irradiance of 0.3.

The air-water surface is simulated for a wind speed of 5 m s^{-1}.

The water column is supposed infinitely deep (no bottom reflection), and inelastic scattering processes are not considered.

The results of these simulations are presented in Fig. 4, which plots the ratio of nadir water-leaving reflectance ratios $\alpha = \rho_{\mathrm{w}}(778.5)/\rho_{\mathrm{w}}(864.8)$ against $\rho_{\mathrm{w}}(864.8)$, thus showing the variation of the ratio for increasing TSM (or b_{b}). Further ratios are plotted on this figure to assess the validity of the various component assumptions underlying Eq. 18. For comparison with the simple theory, a reference value of

$$\alpha_0 = \frac{a_{\mathrm{w}}(864.8)}{a_{\mathrm{w}}(778.5)}\left(\frac{778.5}{864.8}\right)^{-0.15} = 1.72 \quad (21)$$

is defined from Eq. 18. A number of interesting features are seen in Fig. 4a. For very clear waters with reflectance at 864.8 nm less than 10^{-4}, α is significantly greater than α_0 because the backscatter of pure water is important and has a stronger wavelength variation than particulate backscatter.
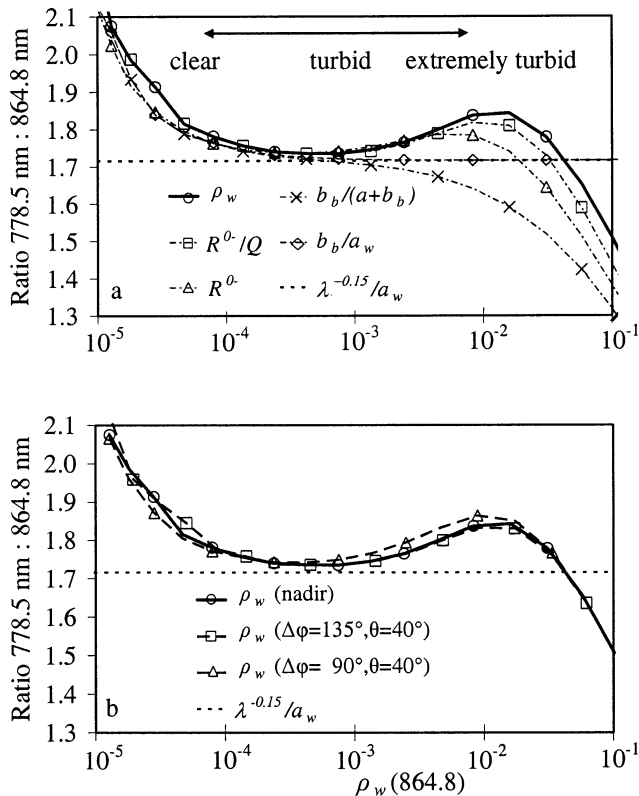
Fig. 4. (a) The 778.5 nm : 864.8 nm ratio from the radiative transfer simulations is plotted against $\rho_w(864.8)$ for the following parameters: ρ_w (at nadir), $R^{0-}:Q$, R^{0-}, $b_b:(a+b_b)$, $b_b:a_w$, and $\lambda^{-0.15}:a_w$. The first of these ratios is α, the last is α_0. The difference between the ρ_w and $b_b:(a+b_b)$ ratios corresponds to the wavelength variation of $f'\mathfrak{R}/Q$ of which the f' variation is the most important. (b) As (a), but plotting the ratios of the following parameters: ρ_w (at nadir), $\rho_w(\Delta\phi = 135°, \theta = 40°)$, and $\rho_w(\Delta\phi = 90°, \theta = 40°)$ to show bidirectional variation.

For moderately turbid waters with 864.8 nm reflectance between 10^{-4} and 10^{-3}, α varies little (between 1.73 and 1.76) and is similar to α_0. For very turbid waters with reflectance between 10^{-3} and 10^{-2}, variation of α from the reference value of α_0 becomes more noticeable (between 1.74 and 1.84). For extremely turbid waters with reflectance greater than 10^{-2}, the variation of α with reflectance becomes significant and the simple theoretical model Eq. 9, or similarly based alternatives (Li 2003), are unreliable. For the range of reflectances from 10^{-4} to 10^{-2}, the water-leaving reflectance ratio is seen to vary with increasing reflectance similarly to both the ratio of subsurface radiance reflectance, R^{0-}/Q^{0-}, and the ratio of subsurface irradiance reflectance, R^{0-}, but surprisingly in an opposite way to the ratio of $b_b/(a + b_b)$. This indicates that departure of α from α_0 in this range can be attributed primarily to a varying wavelength ratio of the parameter f' for increasing reflectance, and that a model based on $b_b/(a + b_b)$ is not appropriate for the range of 864.8 nm reflectances from 10^{-3} to 10^{-2} (see also a discussion of this approximation by Sydor et al. 2004).

Thus, in conclusion, the full radiative transfer simulations presented in this section suggest that the ratio of ρ_w at two NIR wavelengths, and hence the similarity spectrum

$\rho_{wn\,780}(\lambda)$ in general, can be expected to vary slightly: $\pm 5\%$, with reflectance itself over the range of 780 nm reflectances from 10^{-4} to 10^{-1} (corresponding here to total suspended matter concentrations between about 0.3 g m^{-3} and 200 g m^{-3}) of most interest to the turbid water atmospheric correction problem. The simple model of Eq. 18 becomes less reliable at higher reflectances ($>10^{-2}$), corresponding to extremely turbid water. It has been previously shown for laboratory data (Moore et al. 1999) that as 864.8 nm reflectance increases above 10^{-2}, α becomes closer to unity. For very clear water the backscatter of pure water becomes important and the simple model of Eq. 18 must be adjusted to account for a different n.

Bidirectional effects: The simulations of the previous section are used here also to assess bidirectional variation of the similarity spectrum. Thus, in Fig. 4b the reflectance ratio at nadir is compared with the same ratio for zenith viewing angle of $\theta = 40°$ and azimuth viewing relative to the sun of $\Delta\phi = 135°$ (away from the reflected sun, the geometry used for above-water reflectance measurements) and for $\theta = 40°$, $\Delta\phi = 90°$. Although reflectance at a fixed wavelength may vary considerably with viewing direction (up to 10% for these directions in these simulations), the variation of the reflectance ratio varies little. The bidirectional variation over the range of 864.8 nm reflectances from 10^{-4} to 10^{-2} with respect to nadir viewing is $<1\%$ and $<2\%$ for $\Delta\phi = 135°$ and $\Delta\phi = 90°$, respectively.

Experimental Method

Algorithms for atmospheric correction in turbid waters generally use a model similar to that of Eq. 16 together with tabulated data for $a_w(\lambda)$ obtained by laboratory measurements. However, this approach contains uncertainties associated with the model approximations and with the laboratory measurements that will affect the accuracy of the atmospheric correction. In the present study the NIR water-leaving reflectance model of Eq. 18 is tested using seaborne reflectance measurements. This provides a validation of the model which is independent of the laboratory measurements of $a_w(\lambda)$ and which takes into account the difference between nature and the simplified theory.

Test region—Above-water reflectance measurements were made from the oceanographic research vessels *Belgica* (51 m) and *Zeeleeuw* (56 m) during 17 cruises (47 days, 188 stations) in the period 2001–2003 (March–September each year). These cruises were carried out in the southern North Sea, primarily in Belgian coastal waters as shown in Fig. 5, for a range of meteorological and oceanographic conditions as summarized in Table 1. This region is relatively shallow and subject to strong resuspension of various types of bottom sediments from tide- and wind-driven currents. Patterns of high TSM can be clearly seen at NIR wavelengths, even from top-of-atmosphere remote sensing data (Ruddick et al. 2000), making this region particularly suitable for the validation of the turbid water atmospheric correction of ocean color sensors. The water column is generally well-mixed vertically by the turbulence caused by strong tide- and wind-
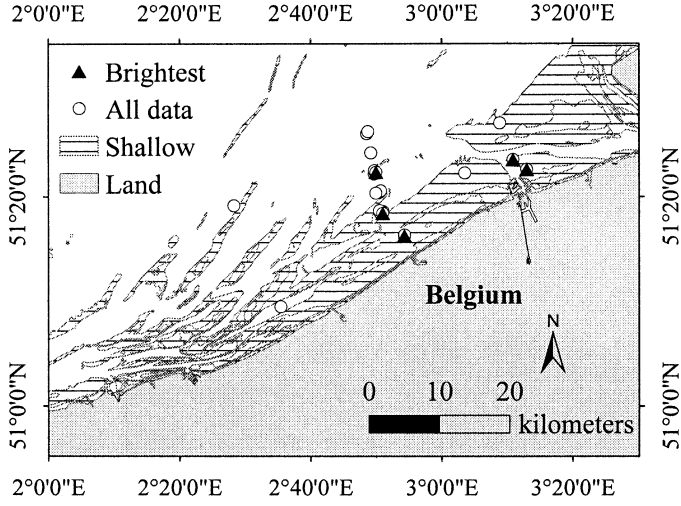
Fig. 5. Location of seaborne reflectance measurements in the southern North Sea. Shallow water (<10 m) is shown as the hatched area. Circles show the location of 26 of the 27 spectra used (some of which are for the same location but on different days), and triangles show the location of the six brightest of these. One further spectrum was measured in English coastal water (off the map).

Table 1. Summary of conditions for seaborne measurements.

	All spectra min–max (median)	Brightest spectra min–max (median)
Number	27	6
Sun zenith (degrees)	28.3–60.2 (44.4)	36.7–60.2 (52.2)
Water depth (m)	10.3–32.0 (15.1)	10.3–24.9 (13.0)
Wind (m s^{-1})	0.0–9.3 (3.6)	1.1–9.3 (7.2)
Sea temperature (°C)	9.1–19.8 (18.5)	9.1–19.0 (17.4)
Practical salinity	29.5–34.5 (31.9)	29.5–31.9 (31.7)
Wave height (m)	0.1–1.5 (0.3)	0.2–1.5 (0.8)
Cloud cover (out of 8)	0–6 (2)	0–5 (3)
Secchi depth (m)	0.5–4.9 (1.8)	0.5–1.0 (0.6)
TSM (g m^{-3})	5.0–81.2 (14.4)	28.6–81.2 (35.3)
Chl *a* (mg m^{-3})	0.4–41.9 (5.5)	5.1–41.9 (7.3)

driven currents and is sufficiently turbid so that bottom reflectance is not visible at the surface for the locations where measurements were made.

Measurement technique and instrumentation—Water-leaving reflectance is calculated from simultaneous above-water measurements of downwelling irradiance, E_d^{0+}; total upwelling radiance (i.e., from the water and from the air-sea interface) at a zenith angle of 40°, L_{sea}^{0+}; and sky radiance, L_{sky}^{0+}, in the direction of the region of sky that reflects into the sea-viewing sensor, by

$$\rho_w = \pi \frac{L_{sea}^{0+} - \rho_{sky}L_{sky}^{0+}}{E_d^{0+}} \quad (22)$$

where ρ_{sky} is the air-water interface reflection coefficient for radiance equal to the Fresnel reflection coefficient in the case of a flat sea surface. This corresponds to "Method 1" of the NASA protocols (Mueller et al. 2000). The air-sea interface reflection coefficient is expected to vary strongly with wind speed for clear sky conditions because of reflection of brighter parts of the sky in the case of higher waves (Mobley 1999), but is approximately independent of wind speed for cloudy conditions. This can be accounted for by switching between clear sky (Eq. 23) and cloudy sky (Eq. 24) models for ρ_{sky}, according to the ratio L_{sky}^{0+}/E_d^{0+} at 750 nm, which takes a value of about 0.02 in the clear sky simulations of Mobley (1999) but can reach much higher values (e.g., of order 0.3 for fully overcast conditions):

$$\rho_{sky} = 0.0256 + 0.00039W$$
$$+ 0.000034W^2 \quad \text{for } \frac{L_{sky}^{0+}(750)}{E_d^{0+}(750)} < 0.05 \quad (23)$$

$$\rho_{sky} = 0.0256 \quad \text{for } \frac{L_{sky}^{0+}(750)}{E_d^{0+}(750)} \geq 0.05 \quad (24)$$

The sunny sky formula of Eq. 23 is derived as a function of wind speed W in meters per second at height 10 m from the model simulations of Mobley (1999) based on the wave slope statistics of Cox and Munk (1954). Although Mobley (1999) reports a slight sun zenith angle dependency for ρ_{sky}, Eq. 23 fits all simulations for the range $30° \leq \theta_0 \leq 70°$ to within 1% for $W = 5$ m s^{-1} and to within 3% for $W = 10$ m s^{-1}. It is noted that for the intermediate case of partially cloudy skies, whether obscuring the sun or patchy near the sky-viewing direction, neither of these formulations is entirely appropriate. Although problematic for many above-water reflectance measurements, this intermediate case is not relevant to the present study because such data are removed from the analysis, as are the fully cloudy data where measurement uncertainties are more significant.

Measurements were performed with three TriOS-RAMSES hyperspectral spectroradiometers, two measuring radiance and one measuring downwelling irradiance. The instruments were mounted on a steel frame (Hooker and Lazin 2000) as shown in Fig. 6. Zenith angles of the sea- and sky-viewing radiance sensors were 40°. The frame was fixed to the prow of the ship, facing forward to minimize ship shadow and reflection (Hooker and Morel 2003). The ship was maneuvered on station to point the radiance sensors at a relative azimuth angle of 135° away from the sun. Lenses were checked and, if necessary, cleaned prior to each measurement. Measurements were made for 10 min, taking a scan of the three instruments every 10 s. The sensors measured over the wavelength range of 350–950 nm with a sampling interval of approximately 3.3 nm and a spectral width of about 10 nm. Position was measured simultaneously by global positioning system (GPS). Data were acquired with the TriOS GmbH MSDA software using the file recorder function and radiometrically calibrated using nominal calibration constants. Calibrated data for E_d^{0+}, L_{sea}^{0+}, and L_{sky}^{0+} were interpolated to 2.5 nm intervals and exported to Microsoft Excel for further processing. The sensors were calibrated in a MERIS Validation Team laboratory every year, after which the definitive spectra were obtained. Details of the data processing, including scan selection and averaging and quality control, are described in Web Appendix 1 (http:// www.aslo.org/lo/toc/vol_51/issue_2/1167a1.pdf). Only data for stations with sunny sky, wind speed <10 m s^{-1}, and low
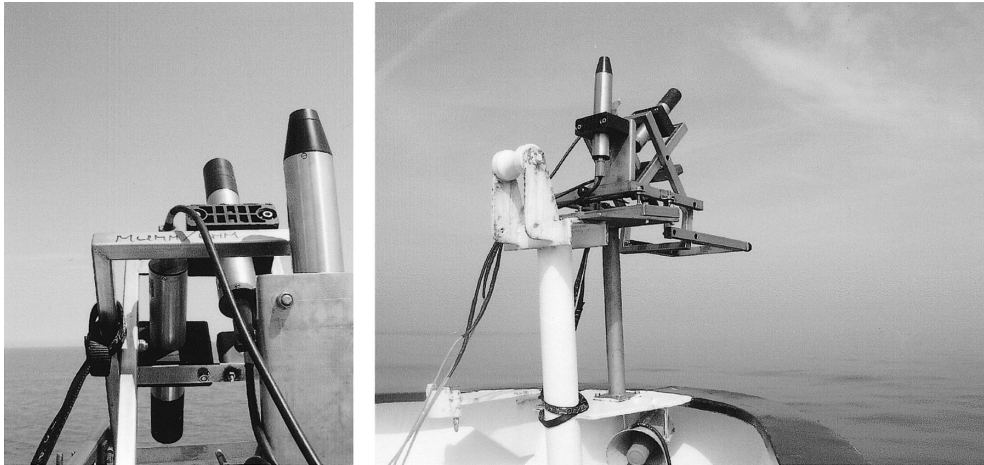
Fig. 6. Frame with three Trios-RAMSES hyperspectral radiometers as installed on the research vessel *Belgica.*

temporal variability have been retained (27 out of 188 stations).

An estimation of measurement uncertainties is given in Web Appendix 2 (http://www.aslo.org/lo/toc/vol_51/issue_2/1167a2.pdf). This shows that the air-sea interface correction gives an absolute uncertainty that is independent of the water reflectance and, thus, is correspondingly larger in relative terms for low reflectances.

Results

The NIR similarity reflectance spectrum—The water-leaving reflectance spectra (400–900 nm) from the 27 selected stations are shown in Fig. 7. Most spectra have a peak between 550 and 600 nm and a distinct slope from 400 to 550 nm, indicating high absorption from colored dissolved organic matter (CDOM) or nonalgae particles. Differences in spectral shape between 650 and 700 nm can be attributed to varying absorption (and possibly also fluorescence) from phytoplankton. Although the magnitude of reflectance varies over one order of magnitude, it is noted that very clear, blue water spectra are not retained in the current data set owing partly to the region sampled, but also to the criteria applied
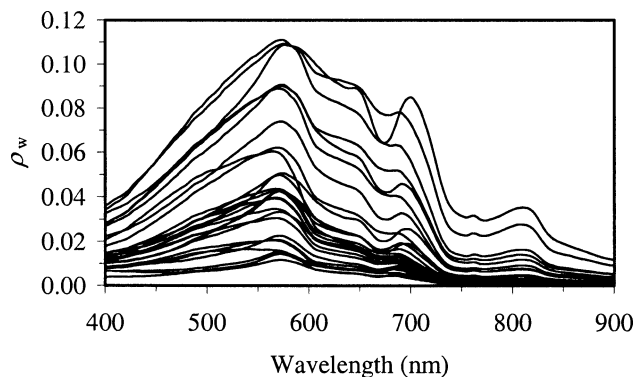

Fig. 7. Measured water-leaving reflectance spectra (400–900 nm) for 27 spectra.

for selection of data: the uncertainty analysis of Web Appendix 2 shows that the air-sea interface correction will give severe degradation of measurements for the clearer waters.

The normalized water-leaving reflectance spectra $\rho_{wn\,780}(\lambda)$ for 650–900 nm from the 27 selected stations are shown in Fig. 8. As expected from the simplified theory, the shape of the reflectance spectra is almost invariant in the spectral range 710–900 nm. As shown in Web Appendix 2, the absolute uncertainty for measurement of ρ_w associated with correction for air-sea interface reflection is independent of ρ_w itself and, hence, the uncertainty of $\rho_{wn\,780}$ decreases rapidly with increasing ρ_w. Thus, calculation of a mean similarity spectrum $\bar\rho_{wn\,780}(\lambda)$ has been made from the mean average subset of the six brightest spectra for which $\rho_w(780) > 0.007$. This mean similarity reflectance spectrum $\bar\rho_{wn\,780}(\lambda)$ is superimposed on Fig. 8 as a solid black line enclosed by dashed black lines indicating the standard deviation. The spread of all 27 spectra in Fig. 8, for example at 820 nm, is much greater than the standard deviation over the six brightest as a result of the greater measurement uncertainty. Interestingly, this spread is systematically below the $\bar\rho_{wn\,780}(\lambda)$ spectrum between 780 and 830 nm and above $\bar\rho_{wn\,780}(\lambda)$ between 830 and 900 nm.

The $\bar\rho_{wn\,780}(\lambda)$ similarity spectrum is tabulated at 2.5 nm intervals in Table 2 and plotted in Fig. 9 against the model of Eq. 18. Such comparison between laboratory pure water absorption measurements and seaborne reflectance measurements has only rarely been attempted previously (Sydor et al. 2002), and the agreement here is strikingly good throughout the range 750–900 nm despite the difficulties involved in both measurement methods and possibly temperature variations for the seaborne data set. Differences for the range 720–750 nm might be caused by temperature difference, extra absorbing components, or simply measurement uncertainties in one or another data set. The local maximum seen at 760 nm for the seaborne measurements is clearly associated with atmospheric oxygen absorption. Here the use of different spectroradiometers for measurement of E_d^{0+} and L_{sea}^{0+} with slightly different central wavelengths and spectral
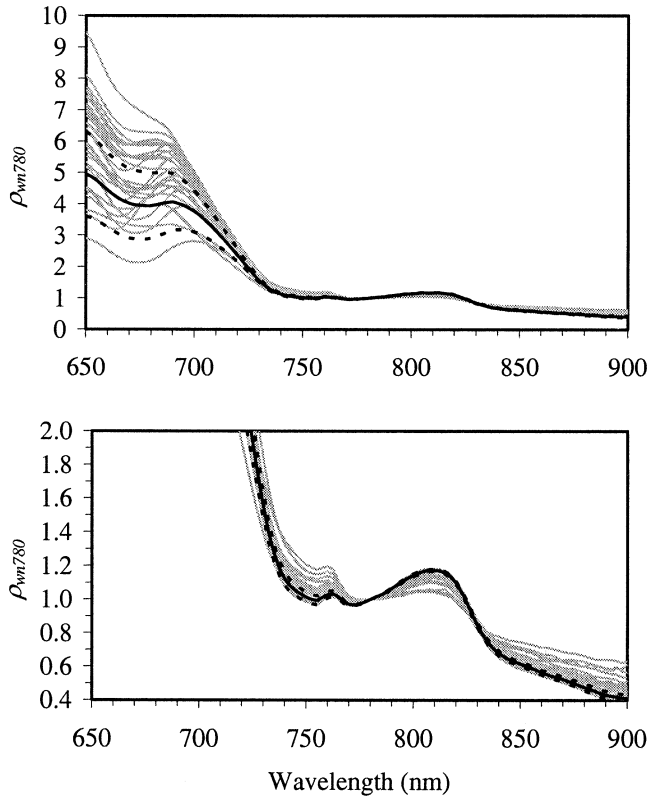
Fig. 8. Measured water-leaving reflectance spectra normalized by reflectance at 780 nm (using different scales for axes) for the 27 spectra considered. The average of the six brightest measurements, the similarity spectrum $\bar{\rho}_{\mathrm{wn}\,780}(\lambda)$, is shown as a thick black line, with standard deviation over these six measurements indicated by the thick dashed lines.

response functions means that features with spectral width smaller than the instrument spectral response width (~ 10 nm) can be distorted and measurements near 760 nm cannot be trusted. Blips of various magnitude and sign near 760 nm can also be seen in reflectance spectra by some other investigators (Schalles et al. 1998; Brando and Dekker 2003; Dall'Olmo and Gitelson 2005), although a very careful quantification of data and analysis of measurement protocol, data processing, and instrument characteristics would be necessary for a full explanation. Differences between the similarity spectrum derived from the Kou et al. (1993) water absorption data (at 22°C and with $n = 0$) and the present seaborne measurements are <5% for the range 770–855 nm and <8% for the range 855–900 nm. These differences are slightly larger than, but of the same order of magnitude as, the estimated measurement uncertainty for the seaborne $\bar{\rho}_{\mathrm{wn}\,780}(\lambda)$ spectrum (see Web Appendix 2).

Reflectance ratios for ocean color sensors—Using the data of Table 2, reflectance ratios for the atmospheric correction bands of existing ocean color sensors are given in Table 3. This table gives both the ratio as calculated directly from Table 2 by interpolating to the central wavelengths as well as a band-weighted ratio. For the latter, the weighted reflectance, $\rho_{\mathrm{w}}(Bi)$, for band i is calculated by integrating spec-

trally using the product of the spectral response function, $\omega_i(\lambda)$, and a downwelling irradiance spectrum, $E_{\mathrm{d}}^{\mathrm{ref}}(\lambda)$, computed by MODTRAN for a 1976 U.S. Standard atmosphere model (zenith sun):

$$\rho_{\mathrm{w}}(Bi) = \frac{\displaystyle\int_{650\ \mathrm{nm}}^{950\ \mathrm{nm}} \omega_i(\lambda)E_{\mathrm{d}}^{\mathrm{ref}}(\lambda)\rho_{\mathrm{wn}\,780}(\lambda)\ d\lambda}{\displaystyle\int_{650\ \mathrm{nm}}^{950\ \mathrm{nm}} \omega_i(\lambda)E_{\mathrm{d}}^{\mathrm{ref}}(\lambda)\ d\lambda} \tag{25}$$

The response functions were obtained from the web sites devoted to each sensor.

As an example of variability of a ratio over the measurement set, a scatterplot of measured reflectances at the MERIS atmospheric correction bands at 778.5 and 864.8 nm is shown for all 27 spectra in Fig. 10, and the reflectance ratio is plotted against reflectance in Fig. 11. Greater scatter of the reflectance ratio is seen for lower reflectances with a suggestion again of a slightly lower $\rho_{\mathrm{w}}(778.5)/\rho(864.8)$ for some lower reflectance spectra. This may result from measurement errors; hence the choice of only the brightest six spectra for calculation of the similarity spectrum $\bar{\rho}_{\mathrm{wn}\,780}(\lambda)$.

If the high uncertainty of the low reflectance points are removed from Figs. 10 and Fig. 11, the remaining points suggest that the first-order theory of Eqs. 16 or 18 is very reliable over the reflectance range considered from 0.002 to 0.035. In fact, there is no clear indication of the second-order effects found in the radiative transfer simulations (Fig. 4a) and found previously in laboratory reflectance measurements by Moore et al. (1999), because the present measurements, unlike the data of Moore et al. (1999), were made for reflectances lying within the range where Fig. 4a shows almost constant α. Any validation by measurements of hypotheses (Whitlock et al. 1981; Li 2003; Sydor et al. 2004) regarding the impact of such second-order effects on NIR reflectance ratios would require even more reflective water than was measured here.

Discussion

The results presented here support the hypothesis of a universal or similarity spectrum for water-leaving reflectance in the near infrared. This hypothesis had been previously suggested by simple optical theory and using data from laboratory measurements of pure water absorption, but only rarely (Sydor et al. 2002) tested using seaborne reflectance measurements. The similarity spectrum hypothesis is discussed theoretically and tested in detail here using both seaborne reflectance measurements and full radiative transfer simulations. Comparison between spectra derived from laboratory pure water absorption measurements and the seaborne reflectance measurements (Fig. 9) shows agreement to within a few percent for the range 730–900 nm. Possible causes of variability from this similarity spectrum have been assessed theoretically and by radiative transfer simulations. The similarity spectrum is shown to be valid for a wide range of turbidities, roughly given by reflectances at 780 nm ranging from 0.0001 to 0.1, corresponding approximately to total suspended matter concentrations ranging from 0.3 to

Table 2. Average similarity reflectance spectrum $\bar{\rho}_{wn\,780}(\lambda)$ calculated from the brightest six seaborne measurements and the standard deviation, σ, over the six measurements. Entries where the standard deviation exceeds 10% of the mean and within 6 nm of 762 nm (see text) are given in italics as less reliable.

λ (nm)	$\bar{\rho}_{wn\,780}$	σ	$\dfrac{\sigma}{\bar{\rho}_{wn\,780}}$	λ (nm)	$\bar{\rho}_{wn\,780}$	σ	$\dfrac{\sigma}{\bar{\rho}_{wn\,780}}$	λ (nm)	$\bar{\rho}_{wn\,780}$	σ	$\dfrac{\sigma}{\bar{\rho}_{wn\,780}}$
650.0	*4.953*	*1.349*	*0.272*	750.0	1.013	0.028	0.028	850.0	0.616	0.012	0.020
652.5	*4.858*	*1.312*	*0.270*	752.5	1.001	0.027	0.027	852.5	0.603	0.012	0.020
655.0	*4.734*	*1.270*	*0.268*	755.0	0.994	0.026	0.026	855.0	0.592	0.012	0.021
657.5	*4.586*	*1.226*	*0.267*	*757.5*	*1.012*	*0.023*	*0.023*	857.5	0.579	0.013	0.022
660.0	*4.432*	*1.188*	*0.268*	*760.0*	*1.029*	*0.022*	*0.021*	860.0	0.564	0.013	0.024
662.5	*4.293*	*1.159*	*0.270*	*762.5*	*1.033*	*0.018*	*0.018*	862.5	0.553	0.013	0.024
665.0	*4.177*	*1.139*	*0.273*	*765.0*	*1.016*	*0.014*	*0.013*	865.0	0.544	0.015	0.028
667.5	*4.082*	*1.125*	*0.276*	*767.5*	*0.985*	*0.009*	*0.009*	867.5	0.534	0.016	0.030
670.0	*4.017*	*1.112*	*0.277*	770.0	0.971	0.007	0.007	870.0	0.523	0.016	0.031
672.5	*3.976*	*1.099*	*0.276*	772.5	0.968	0.005	0.005	872.5	0.512	0.016	0.031
675.0	*3.949*	*1.084*	*0.274*	775.0	0.972	0.003	0.003	875.0	0.501	0.018	0.035
677.5	*3.939*	*1.065*	*0.271*	777.5	0.985	0.002	0.002	877.5	0.488	0.019	0.038
680.0	*3.937*	*1.041*	*0.264*	780.0	1.000	0.000	0.000	880.0	0.476	0.021	0.043
682.5	*3.974*	*1.018*	*0.256*	782.5	1.015	0.001	0.001	882.5	0.465	0.022	0.047
685.0	*4.016*	*0.988*	*0.246*	785.0	1.029	0.002	0.002	885.0	0.454	0.021	0.046
687.5	*4.046*	*0.949*	*0.234*	787.5	1.046	0.004	0.004	887.5	0.440	0.021	0.048
690.0	*4.061*	*0.901*	*0.222*	790.0	1.067	0.005	0.005	890.0	0.431	0.022	0.051
692.5	*4.015*	*0.842*	*0.210*	792.5	1.087	0.006	0.006	892.5	0.425	0.022	0.052
695.0	*3.948*	*0.782*	*0.198*	795.0	1.108	0.008	0.007	895.0	0.419	0.023	0.054
697.5	*3.862*	*0.720*	*0.186*	797.5	1.127	0.008	0.007	897.5	0.413	0.023	0.055
700.0	*3.757*	*0.657*	*0.175*	800.0	1.145	0.009	0.007	900.0	0.409	0.027	0.066
702.5	*3.621*	*0.593*	*0.164*	802.5	1.159	0.009	0.008				
705.0	*3.466*	*0.529*	*0.153*	805.0	1.169	0.009	0.008				
707.5	*3.297*	*0.466*	*0.141*	807.5	1.173	0.006	0.005				
710.0	*3.118*	*0.405*	*0.130*	810.0	1.175	0.007	0.006				
712.5	*2.931*	*0.350*	*0.119*	812.5	1.171	0.008	0.007				
715.0	*2.754*	*0.301*	*0.109*	815.0	1.159	0.007	0.006				
717.5	2.560	0.252	0.098	817.5	1.138	0.009	0.007				
720.0	2.350	0.204	0.087	820.0	1.098	0.009	0.008				
722.5	2.144	0.162	0.075	822.5	1.043	0.010	0.010				
725.0	1.937	0.126	0.065	825.0	0.980	0.013	0.013				
727.5	1.736	0.097	0.056	827.5	0.912	0.015	0.016				
730.0	1.551	0.075	0.048	830.0	0.846	0.015	0.018				
732.5	1.393	0.060	0.043	832.5	0.788	0.016	0.020				
735.0	1.273	0.051	0.040	835.0	0.742	0.015	0.021				
737.5	1.185	0.045	0.038	837.5	0.707	0.014	0.020				
740.0	1.123	0.040	0.036	840.0	0.678	0.013	0.019				
742.5	1.080	0.036	0.033	842.5	0.658	0.013	0.020				
745.0	1.053	0.033	0.031	845.0	0.640	0.013	0.021				
747.5	1.032	0.030	0.029	847.5	0.627	0.013	0.020				

200 g m^{-3}. For very clear waters (e.g., NIR reflectance <0.0001), the spectrum should be modified to account for the different wavelength dependence of backscatter from particles and pure water, although the NIR reflectance in such cases is generally not measurable and for most practical applications can be assumed as zero. For extremely turbid waters (e.g., NIR reflectance >0.1), the similarity spectrum will need to be modified to account for nonlinearity of the relationship between reflectance and backscattering or scattering (Sydor et al. 2004) coefficients.

The results given in Tables 2 and 3 can be used directly to improve the input parameters used for atmospheric correction of ocean color sensors over turbid coastal and inland waters. Further applications of these results, especially Table 2, can be considered for the design of TSM algorithms and

the correction or quality control of above-water reflectance measurements.

Both the mean and standard deviation reported in Table 2 are relevant for the design of TSM algorithms, where the choice of wavelength(s) used for retrieval should be a compromise between the accuracy of satellite-derived waterleaving reflectance (related to atmospheric correction, signal:noise, and calibration issues) and the natural variability of water-leaving reflectance from factors not directly related to TSM such as CDOM absorption or phytoplankton absorption. Quantification of such effects by Table 2 provides input for the design of such algorithms.

For clear case 1 waters it is well established that the hypothesis of zero water-leaving reflectance for NIR wavelengths can be used for correction (Carder and Steward
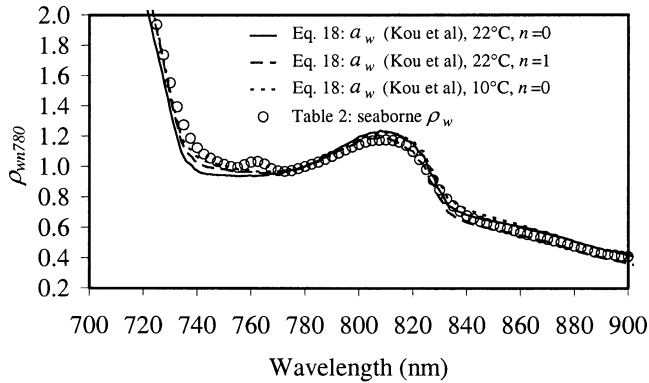
Fig. 9. As Fig. 3, but with the addition of the normalized "similarity" reflectance spectrum, $\bar{\rho}_{wn\,780}(\lambda)$, from seaborne measurements.

Fig. 10. Scatterplot of reflectances at bands used for atmospheric correction of MERIS for 27 measurements. The line $\rho_w(778.5)$ = $1.820 \times \rho_w(864.8)$ derived from the similarity spectrum of Table 2 is superimposed.

1985) or quality control of above-water reflectance measurements (e.g., to detect contamination by ship shadow or reflection; Hooker and Morel 2003). For more reflective waters such a hypothesis is no longer valid. However, using the data of Table 2, it is possible to generalize such methods to more reflective waters. Thus, the required NIR reflectance ratio for two wavelengths could be imposed and the air-sea interface correction adapted until the required fit is obtained, as proposed by Gould et al. (2001) who use data at 715 and 735 nm. Alternatively, if a correction procedure such as that of Eq. 23 is adopted, then the data of Table 2 can be used to control the quality of derived reflectance measurements (e.g., by providing an independent estimate of the entire NIR spectrum from a single wavelength such as 780 nm for comparison with the measured spectrum). For reflectance measurements where high and guaranteed quality is necessary, such as for ocean color sensor validation, the latter approach
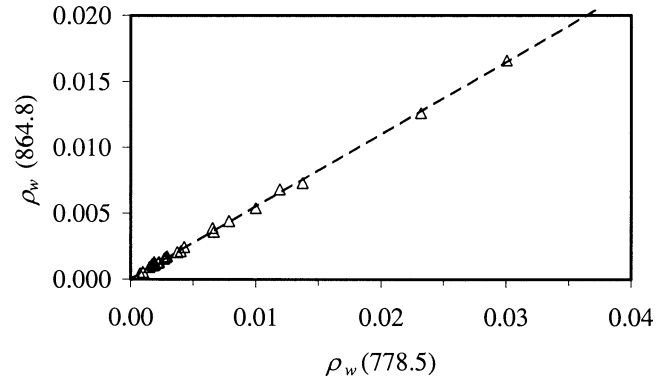
of using the NIR spectrum for quality control seems preferable. This could even be applied for the quality control of almost all remotely sensed water-leaving reflectance spectra, be they from seaborne, airborne, or spaceborne sensors. For other applications (e.g., seaborne data for TSM and Chl a calibration and validation), the former approach may be useful in order to increase the number of usable spectra, although at the expense of losing the possibility of independent information for quality control.

It is clear that the NIR part of the electromagnetic spectrum, and particularly between 710 and 900 nm, offers new perspectives for improvements in optical remote sensing of coastal and inland waters. Only a few measurements are available for inherent optical properties in this spectral range and, in particular, for possible variations of pure water absorption, for example related to temperature. Further mea-

Table 3. Water-leaving reflectance ratios relevant for atmospheric correction of ocean color sensors calculated from seaborne measurements and the pure water absorption spectrum of Kou et al. (1993). The SeaWiFS $\rho_w(B7)$: $\rho_w(B8)$ ratio is not given for the seaborne measurements because of unreliable data near 762 nm.

| Sensor	Band number (center wavelength in nm)	NIR band ratio	Seaborne reflectance measurements		From a_w of Kou et al. (1993)
			From central wavelength	Band-weighted	
SeaWiFS	6 (670)	$\rho_w(B6)$: $\rho_w(B8)$	7.390	7.489	9.705
	7 (765)	$\rho_w(B7)$: $\rho_w(B8)$			1.611
	8 (865)				
MODISTERRA	14 (676.7)	$\rho_w(B14)$: $\rho_w(B16)$	7.318	7.269 (7.387)	9.511
(AQUA)	15 (746.4)	$\rho_w(B15)$: $\rho_w(B16)$	1.932	1.984 (1.945)	1.639
	16 (866.2)				
MERIS	8 (680.9)	$\rho(B8)$: $\rho_w(B13)$	7.258	7.246	9.125
	9 (708.4)	$\rho_w(B9)$: $\rho_w(B13)$	5.936	5.951	5.570
	10 (753.5)	$\rho_w(B10)$: $\rho_w(B13)$	1.833	1.836	1.601
	12 (778.5)	$\rho_w(B12)$: $\rho_w(B13)$	1.820	1.817	1.689
	13 (864.8)				
GLI	12 (679.9)	$\rho_w(B12)$: $\rho_w(B18)$	7.304	7.345	9.311
	14 (710.5)	$\rho_w(B14)$: $\rho_w(B18)$	5.712	5.696	5.286
	16 (749.0)	$\rho_w(B16)$: $\rho_w(B18)$	1.892	1.906	1.634
	18 (866.1)	$\rho_w(B13)$: $\rho_w(B19)$	7.283	7.324	9.361
	13 (678.6)				
	19 (865.7)				
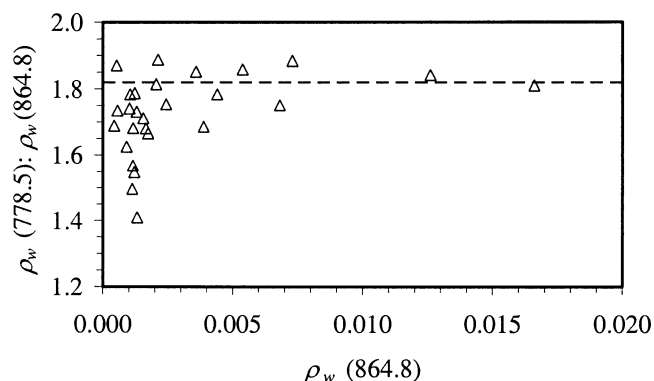
Fig. 11. Scatterplot of $\rho_w(778.5) : \rho_w(864.8)$ against $\rho_w(864.8)$ with the same data as Fig. 10. The line $\rho_w(778.5) : \rho_w(864.8) = 1.820$ derived from the similarity spectrum of Table 2 is superimposed.

surement of NIR IOPs could help improve optical theory, such as that used in this paper, and consequently the basis for atmospheric correction of ocean color data over highly reflective coastal and inland waters. Seaborne, airborne, and spaceborne NIR reflectance measurements for highly reflective waters also need to be expanded and more intensively analyzed, possibly considering also wavelengths such as 1020 or 1380 nm (Hu et al. 2000) sufficiently unaffected by water vapor absorption. Such investigations should certainly be carried out as far as possible in a hyperspectral context to maximize information content. As one example, the oxygen absorption band at 762 nm may, instead of causing problems for atmospheric correction as is the case for SeaWiFS (Hu et al. 2000), provide extra useful information for atmospheric correction or cirrus detection provided sufficient spectral resolution is available nearby. Finally, future work is needed to further improve procedures for above-water reflectance measurements and reduce uncertainties to improve validation of ocean color sensors in highly reflective waters, especially for NIR bands.

References

ALTHUIS, I. J. A., AND S. SHIMWELL. 1995. Modelling of remote sensing reflectance spectra for suspended matter concentration detection in coastal waters. EARSEL Advances in Remote Sensing **4:** 53–59.

BABIN, M., A. MOREL, V. FOURNIER-SICRE, F. FELL, AND D. STRAMSKI. 2003a. Light scattering properties of marine particles in coastal and open ocean waters as related to the particle mass concentration. Limnol. Oceanogr. **28:** 843–859.

———, AND D. STRAMSKI. 2002. Light absorption by aquatic particles in the near-infrared spectral region. Limnol. Oceanogr. **47:** 911–915.

———, ———, G. M. FERRARI, H. CLAUSTRE, A. BRICAUD, G. OBOLENSKY, AND N. HOEPFFNER. 2003b. Variations in the light absorption coefficients of phytoplankton, nonalgal particles and dissolved organic matter in coastal waters around Europe. Journal of Geophysical Research **108:** 3211. [doi:3210.1029/2001JC000882].

BOWERS, D. G., S. BOUDJELAS, AND G. E. L. HARKER. 1998. The distribution of fine suspended sediments in the surface waters of the Irish Sea and its relation to tidal stirring. International Journal of Remote Sensing **19:** 2789–2805.

BRANDO, V. E., AND A. G. DEKKER. 2003. Satellite hyperspectral remote sensing for estimating estuarine and coastal water quality. IEEE Trans. Geosci. Remote Sens. **41:** 1378–1387.

BRICAUD, A., A. MOREL, AND L. PRIEUR. 1981. Absorption by dissolved organic matter of the sea (yellow substance) in the UV and visible domains. Limnol. Oceanogr. **26:** 43–53.

BUITEVELD, H., J. H. M. HAKVOORT, AND M. DONZE. 1994. The optical properties of pure water. Ocean Optics XII. SPIE **2258:** 174–183.

CARDER, K. L., AND R. G. STEWARD. 1985. A remote-sensing reflectance model of a red-tide dinoflagellate off west Florida. Limnol. Oceanogr. **30:** 286–298.

COX, C., AND W. MUNK. 1954. Measurements of the roughness of the sea surface from photographs of the Sun's glitter. Journal of the Optical Society of America **44:** 834–850.

DALL'OLMO, G., AND A. A. GITELSON. 2005. Effect of bio-optical parameter variability on the remote estimation of chlorophyll-*a* concentration in turbid productive waters: Experimental results. Applied Optics **44:** 412–422.

DEKKER, A. G. 1993. Detection of water quality parameters for eutrophic waters by high resolution remote sensing. Ph.D. thesis. ISBN 90-9006234-3. Vrije Universiteit Amsterdam.

DOXARAN, D., J.-M. FROIDEFOND, S. LAVENDER, AND P. CASTAING. 2002. Spectral signatures of highly turbid waters. Application with SPOT data to quantify total suspended matter concentrations. Remote Sens. Environ. **81:** 149–161.

FORGET, P., S. OUILLON, F. LAHET, AND P. BROCHE. 1999. Inversion of reflectance spectra of nonchlorophyllous turbid coastal waters. Remote Sens. Environ. **68:** 264–277.

GITELSON, A. 1992. The peak near 700 nm on radiance spectra of algae and water: Relationships of its magnitude and position with chlorophyll concentration. Int. J. Remote Sens. **13:** 3367–3373.

GONS, H. J. 1999. Optical teledetection of chlorophyll-*a* in turbid inland waters. Environmental Science and Technology **33:** 1127–1133.

GORDON, H. R., O. B. BROWN, R. H. EVANS, J. W. BROWN, R. C. SMITH, K. S. BAKER, AND D. K. CLARK. 1988. A semianalytical radiance model of ocean color. Journal of Geophysical Research **93:** 10909–10924.

———, AND A. Y. MOREL. 1983. Remote assessment of ocean color for interpretation of satellite visible imagery. Springer-Verlag.

———, AND M. WANG. 1994. Retrieval of water-leaving radiance and aerosol optical thickness over the oceans with SeaWiFS: A preliminary algorithm. Applied Optics **33:** 443–452.

GOULD, R. W., R. A. ARNONE, AND P. M. MARTINOLICH. 1999. Spectral dependance of the scattering coefficient in case 1 and case 2 waters. Applied Optics **38:** 2377–2383.

———, ———, AND M. SYDOR. 2001. Absorption, scattering and remote-sensing reflectance relationships in coastal waters: Testing a new inversion algorithm. Journal of Coastal Research **17:** 328–341.

HALE, G. M., AND M. R. QUERRY. 1973. Optical constants of water in the 200nm to 200μm wavelength region. Applied Optics **12:** 555–563.

HAN, L., AND D. C. RUNDQUIST. 1997. Comparison of NIR/red ratio and first derivative of reflectance in estimating algal-chlorophyll concentration: A case study in a turbid reservoir. Remote Sens. Environ. **62:** 253–261.

HOLLIS, V. S. 2002. Non-invasive monitoring of brain tissue temperature by near-infrared spectroscopy. Phd Thesis. University College London.

HOOKER, S. B., AND G. LAZIN. 2000. The SeaBOARR-99 Field Campaign, p. 46. NASA Technical Memorandum 2000-206892, V. 8.

———, AND A. MOREL. 2003. Platform and environmental effects

on above-water determinations of water-leaving radiances. Journal of Atmospheric and Oceanic Technology **20:** 187–205.

Hu, C., K. L. Carder, and F. E. Muller-Karger. 2000. Atmospheric correction of SeaWiFS imagery: Assessment of the use of alternative bands. Applied Optics **39:** 3573–3581.

Kou, L., D. Labrie, and P. Chylek. 1993. Refractive indices of water and ice in the $0.65\,\mu m$ to $2.5\,\mu m$ spectral range. Applied Optics **32:** 3531–3540.

Lavender, S. J., M. H. Pinkerton, G. F. Moore, J. Aiken, and D. Blondeau-Patissier. 2005. Modification to the atmospheric correction of SeaWiFS ocean colour images over turbid waters. Continental Shelf Research **25:** 539–555.

Li, Y. 2003. Atmospheric correction of SeaWiFS imagery for turbid coastal and inland waters: Comment. Applied Optics **42:** 893–895.

Loisel, H., and A. Morel. 2001. Non-isotropy of the upward radiance field in typical coastal (case 2) waters. International Journal of Remote Sensing **22:** 275–295.

Malthus, T. J., and A. G. Dekker. 1995. First derivative indices for the remote sensing of inland water quality using high spectral resolution reflectance. Environ. Int. **21:** 221–232.

Mobley, C. D. 1994. Light and water: Radiative transfer in natural waters. Academic Press.

———. 1999. Estimation of the remote-sensing reflectance from above-surface measurements. Applied Optics **38:** 7442–7455.

———, and L. K. Sundman. 2001. Hydrolight 4.2 technical documentation, p. 79. Sequoia Scientific.

Moore, G. F., J. Aiken, and S. J. Lavender. 1999. The atmospheric correction of water colour and the quantitative retrieval of total suspended matter in case II waters: Application to MERIS. International Journal of Remote Sensing **20:** 1713–1734.

Morel, A. 1974. Optical properties of pure water and sea water, p. 1–24. *In* N. G. Jerlov and E. Steeman-Nielsen [eds.], Optical aspects of oceanography. Academic Press.

———, and B. Gentili. 1991. Diffuse reflectance of oceanic waters: Its dependence on sun angle as influenced by the molecular scattering contribution. Applied Optics **30:** 4427–4438.

———, and ———. 1996. Diffuse reflectance of oceanic waters. III. Implications of bidirectionality for the remote sensing problem. Applied Optics **35:** 4850–4862.

———, and L. Prieur. 1977. Analysis of variations in ocean color. Limnol. Oceanogr. **22:** 709–722.

Mueller, J. L., and others. 2000. Above-water radiance and remote sensing reflectance measurements and analysis protocols, p. 98–107. *In* G. S. Fargion and J. L. Mueller [eds.], Ocean optics protocols for satellite ocean color sensor validation. Revision 2. National Aeronautical and Space Administration.

Palmer, K. F., and D. J. Williams. 1974. Optical properties of water in the near infrared. J. Opt. Soc. America **64:** 1107–1110.

Park, Y., and K. Ruddick. 2005. Model of remote-sensing reflectance including bidirectional effects for case 1 and case 2 waters. Applied Optics **44:** 1236–1249.

Pegau, W. S., G. Gray, and J. R. Zaneveld. 1997. Absorption and attenuation of visible and near-infrared light in water: Dependence on temperature and salinity. Applied Optics **36:** 6035–6046.

———, and J. R. V. Zaneveld. 1993. Temperature-dependent absorption of water in the red and near-infrared portions of the spectrum. Limnol. Oceanogr. **38:** 188–192.

Ruddick, K. G., F. Ovidio, and M. Rijkeboer. 2000. Atmospheric correction of SeaWiFS imagery for turbid coastal and inland waters. Applied Optics **39:** 897–912.

Schalles, J. F., A. T. Sheil, J. F. Tycast, J. J. Alberts, and Y. Z. Yacobi. 1998. Detection of chlorophyll, seston and dissolved organic matter in the estuarine mixing zone of Georgia coastal plain rivers, p. 315–324. 5th International Conference on Remote Sensing for Marine and Coastal Environments. Environmental Research Institute of Michigan.

Smith, R. C., and K. S. Baker. 1981. Optical properties of the clearest natural waters (200–800nm). Applied Optics **20:** 177–184.

Stumpf, R. P., R. A. Arnone, R. W. Gould, P. M. Martinolich, and V. Ransibrahmanakhul. 2002. A partially coupled ocean-atmosphere model for retrieval of water-leaving radiance from SeaWiFS in coastal waters, p. 51–59. Algorithm updates for the fourth SeaWiFS data reprocessing. NASA Technical Memorandum 2003-206892, V. 22.

———, and J. R. Pennock. 1989. Calibration of a general optical equation for remote sensing of suspended sediments in a moderately turbid estuary. Journal of Geophysical Research **94:** 14363–14371.

Sydor, M., R. W. Gould, R. A. Arnone, V. I. Haltrin, and W. Goode. 2004. Uniqueness on remote sensing of the inherent optical properties of ocean water. Applied Optics **43:** 2156–2162.

———, B. D. Wolz, and A. M. Thralow. 2002. Spectral analysis of bulk reflectance from coastal waters: Deconvolution of diffuse spectra due to scattering and absorption by coastal water. Journal of Coastal Research **18:** 352–361.

Tassan, S., and G. M. Ferrari. 1995. Proposal for the measurement of backward and total scattering by mineral particles suspended in water. Applied Optics **34:** 8345–8353.

Tassan, S., and G. M. Ferrari. 2003. Variability of light absorption by aquatic particles in the near-infrared spectral region. Applied Optics **42:** 4802–4810.

Van Der Woerd, H., and R. Pasterkamp. 2004. Mapping of the North Sea turbid coastal waters using SeaWiFS data. Canadian Journal of Remote Sensing **30:** 44–53.

Whitlock, C. H., L. R. Poole, J. W. Usry, W. M. Houghton, W. G. Witte, W. D. Morris, and E. A. Gurganis. 1981. Comparison of reflectance with backscatter and absorption parameters for turbid waters. Applied Optics **20:** 1696–1703.